iScience

CellPress
OPEN ACCESS

Article

Robust Filtering and Noise Suppression in Intragenic miRNA-Mediated Host Regulation

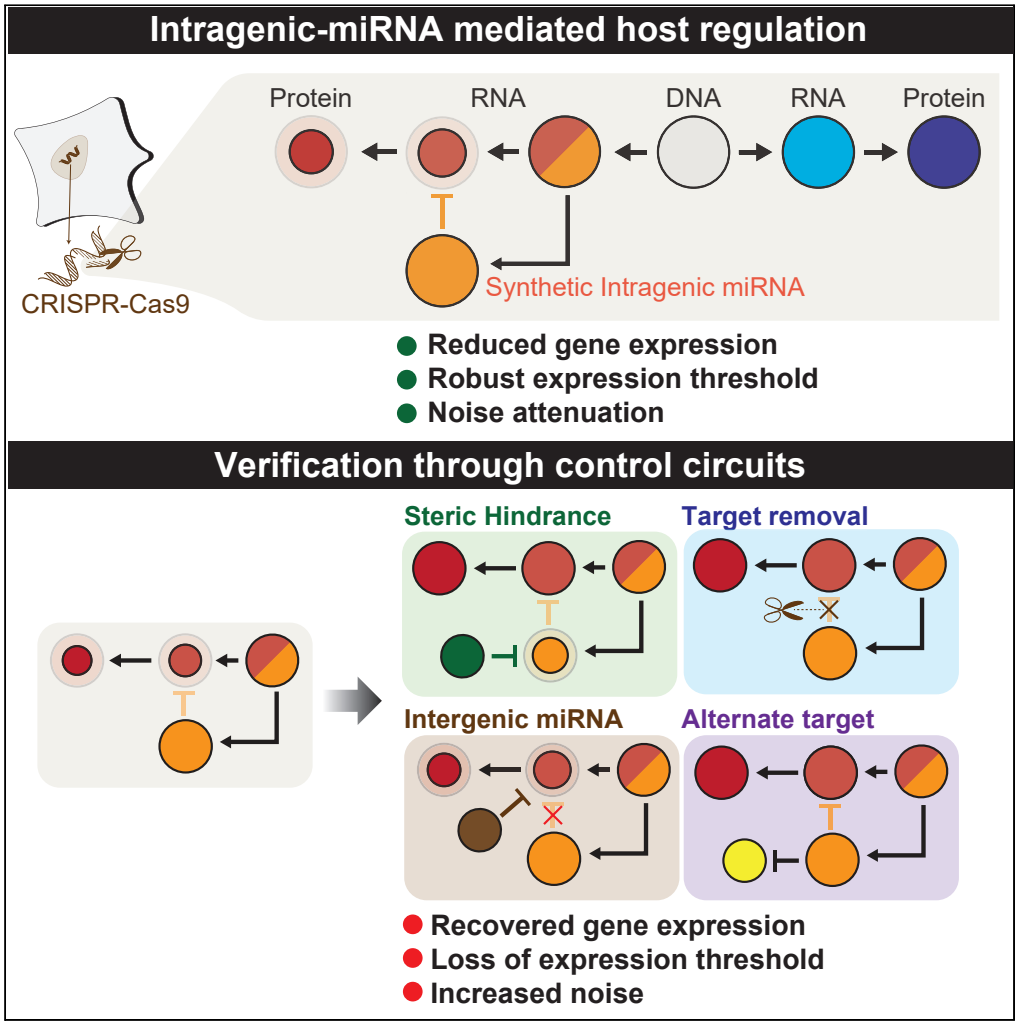

Taek Kang, Tyler Quarton, Chance M. Nowak, Kristina Ehrhardt, Abhyudai Singh, Yi Li, Leonidas Bleris

bleris@utdallas.edu

HIGHLIGHTS

Intragenic miRNA-based host regulation was recreated using a synthetic miRNA

The system was integrated in HEK293 cells via CRISPR-based safe-harbor integration

The system generates a gene expression threshold robust to host promoter strength

Host gene output has reduced noise compared to a splicing-alone architecture

Kang et al., iScience *23*, 101595
October 23, 2020
https://doi.org/10.1016/j.isci.2020.101595

iScience

CellPress
OPEN ACCESS

Article

Robust Filtering and Noise Suppression in Intragenic miRNA-Mediated Host Regulation

Taek Kang,[1,2] Tyler Quarton,[1,2] Chance M. Nowak,[2,4] Kristina Ehrhardt,[1,2] Abhyudai Singh,[3] Yi Li,[1,2] and Leonidas Bleris[1,2,4,5,*]

SUMMARY

MicroRNAs (miRNAs) are short non-coding RNA molecules that regulate gene expression post-transcriptionally by binding to target messenger RNAs (mRNAs). Many human miRNAs are intragenic, located within introns of protein-coding sequence (host). Intriguingly, a percentage of intragenic miRNAs downregulate the host transcript forming an incoherent feedforward motif topology. Here, we study intragenic miRNA-mediated host gene regulation using a synthetic gene circuit stably integrated within a safe-harbor locus of human cells. When the intragenic miRNA is directed to inhibit the host transcript, we observe a reduction in reporter expression accompanied by output filtering and noise reduction. Specifically, the system operates as a filter with respect to promoter strength, with the threshold being robust to promoter strength and measurement time. Additionally, the intragenic miRNA regulation reduces expression noise compared to splicing-alone architecture. Our results provide a new insight into miRNA-mediated gene expression, with direct implications to gene therapy and synthetic biology applications.

INTRODUCTION

MicroRNAs (miRNAs) are a class of short, 17- to 22-nucleotide, non-coding RNA, which regulate gene expression through sequence complementarity (Bartel, 2004; Kim and Kim, 2007). Approximately half of miRNA genes can be found in intergenic regions (between genes) (Table S1), whereas the intragenic miRNAs (inside genes) are predominantly located inside host gene introns and usually oriented on the same DNA strand of the "host" pre-mRNA which gives rise to both exon and intragenic miRNA (He et al., 2012; Hinske et al., 2010; Lee et al., 2004). Intergenic miRNA genes present their own promoter region (Lee et al., 2004; Rodriguez et al., 2004; Ying and Lin, 2006), while same-strand intragenic miRNAs are co-transcribed with their host gene (He et al., 2012; Hinske et al., 2010; Ma et al., 2011) and then processed to become mature, functional miRNAs. While each intergenic miRNA is considered for its own unique transcriptional unit and expression pattern, it is believed that mechanisms which regulate the production of intragenic miRNAs follow that of its host gene (Baskerville and Bartel, 2005). One hypothesis is that intragenic miRNAs support the host gene by silencing genes antagonistic to itself or by coordinating the expression of genes related to the host gene (Dill et al., 2012; Hinske et al., 2014; Lutter et al., 2010).

Intragenic miRNAs can regulate their host genes via complementary targets present in their 3′ untranslated region (3′ UTR) (Flynt and Lai, 2008; Li et al., 2007), forming an incoherent feedforward loop (IFFL) (Alon, 2006; Bleris et al., 2011; Bosia et al., 2012; Mangan and Alon, 2003; Osella et al., 2011a) regulatory mechanism, as mRNA splicing and miRNA processing occur before miRNA-based repression (Figure 1A). More than half of known miRNAs have been predicted to be intragenic and are implicated in a wide array of biological processes from development to cancer biogenesis (Hinske et al., 2014; Lutter et al., 2010). In particular, two cases of intragenic miRNA-mediated host gene regulation that have been experimentally studied are miR-26b and miR-128, both of which are involved in critical processes in cancer proliferation and neural development, respectively (Dill et al., 2012; Li et al., 2013).

We previously characterized transcriptional and post-transcriptional IFFL motifs in transient transfection experiments in cultured human cells and have shown that the IFFL motif leads to adaptation in genetic

[1]Bioengineering Department, University of Texas at Dallas, Richardson, TX 75080, USA

[2]Center for Systems Biology, University of Texas at Dallas, Richardson, TX 75080, USA

[3]Department of Electrical Engineering, University of Delaware, Newark, DE 19716, USA

[4]Department of Biological Sciences, University of Texas at Dallas, Richardson, TX 75080, USA

[5]Lead Contact

*Correspondence: bleris@utdallas.edu

https://doi.org/10.1016/j.isci.2020.101595

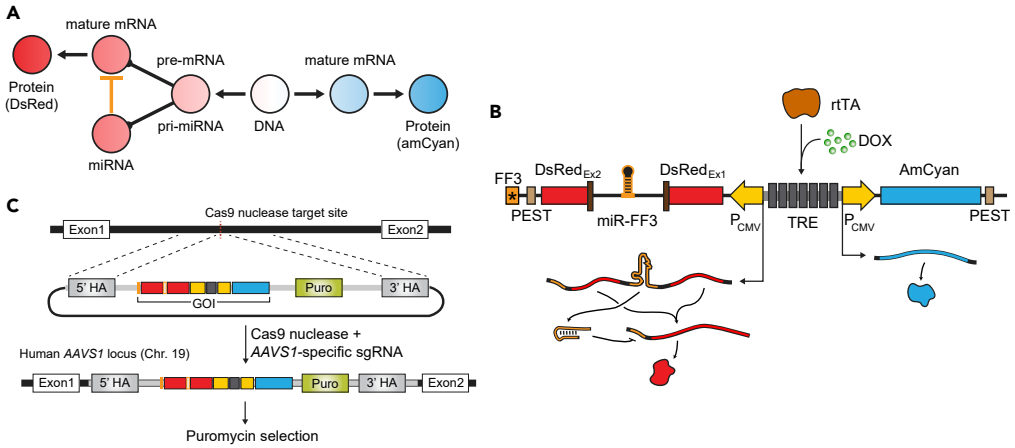

Figure 1. Modeling the Host-Transcriptional Regulation by Intragenic miRNA

(A–C) (A) Graphical representation of the synthetic gene circuit, (B) schematic of the corresponding plasmid, and (C) the CRISPR-Cas9-mediated genomic integration strategy. (A) The synthetic circuit models an intragenic miRNA-mediated transcriptional regulation; the nascent transcript for dsRed fluorescent protein functions as a pre-mRNA as well as a pri-miRNA. (B) The synthetic gene circuit consists of a Tetracycline-controlled promoter (Tet-On) flanked by two different fluorescent reporter genes (AmCyan and dsRed). To introduce an artificial intron in dsRed, a fragment containing synthetic miRNA FF3 flanked by splice sites are inserted in the middle of the coding sequence. The 3′ end of the dsRed gene is added with PEST tag to reduce protein half-life and the FF3 miRNA target. (C) The synthetic construct is stably integrated in HEK293 genome in AAVS1 locus via sgRNA/SpCas9-targeted DNA cleavage and subsequent homologous recombination. Puromycin resistance was included in the synthetic gene circuit to aid in selection for isogenic clones.

template fluctuations (Bleris et al., 2011). Herein, we investigate the properties of intragenic miRNA-mediated host gene regulation using single-copy genetic circuits stably integrated in human kidney cells. Our results show this regulatory motif acts as a filter with respect to promoter strength, preventing gene expression below a threshold that is robust to promoter strength and measurement time. Moreover, cells with active expression have reduced noise compared to a splicing-alone architecture.

RESULTS

Construction and Characterization of Synthetic Circuit

To engineer a system that implements intragenic miRNA-mediated host gene control, we adopted a two-reporter circuit (Kashyap et al., 2013; Shimoga et al., 2013) that is based on a single inducible bidirectional promoter with TET Response Element (TRE). The left fluorescent reporter-coding sequence (DsRed express) was modified with two consensus splice sites such that the transcript produces two exons surrounding a single intron before splicing (Figure 1B). Within the artificial intron, we cloned a synthetic miRNA (namely miRNA FF3 [Bleris et al., 2011; Leisner et al., 2010]). Notably, the FF3 target does not have cross talk within the cell (Rinaudo et al., 2007). A single copy of the fully complementary FF3 miRNA target site (Figure S1) was cloned to the 3′ UTR of the edited DsRed express-coding sequence. The resulting transcript serves both as a pre-mRNA and a pri-miRNA; after splicing, the exon is ready to be translated, while the intron will undergo endogenous processing to become a mature miRNA. The other reporter gene (AmCyan) is unaltered, and thus, its nascent mRNA transcript is translated normally without interruption. To ensure that the fluorescent reporter does not build up excessively, a PEST tag was added to the C-terminal end of both reporters to accelerate protein degradation (Figure 1B).

The synthetic circuit was then stably integrated in HEK293 cells that constitutively produce rtTA, which enables the circuit to be activated by doxycycline (Dox). We integrated the cassette into the AAVS1 safe-harbor locus to minimize epigenetic interference and cross talk with other genes or regulatory elements (Sadelain et al., 2012; Satoh et al., 2000). The integration of the transgene cargo was performed using CRISPR/SpCas9 (Hsu et al., 2014; Qi et al., 2013) with a single guide RNA specific to the AAVS1 locus (Figure 1C and Table S2). In addition to the circuit, the donor plasmid contains the puromycin resistance gene as a selection marker. After integration, we isolated single cells via serial dilution under selection to generate monoclonal populations with the intragenic miRNA cassette (Transparent Methods and Table

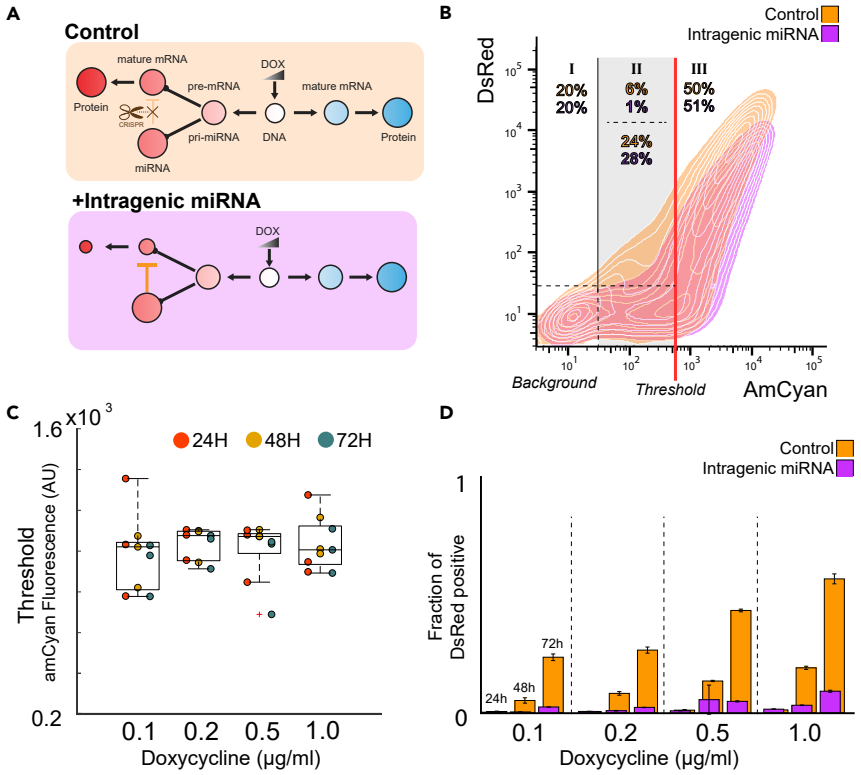

Figure 2. Filtering of dsRed Fluorescent Activity by Intragenic miRNA

(A) Schematic representation of the control gene circuit with no transcriptional repression to either fluorescent reporters (top) and the circuit with active intragenic miRNA-controlled dsRed (bottom).

(B) The threshold for dsRed expression in our genetic circuit is defined as the promoter activity level (as measured by AmCyan fluorescence) at which the dsRed expression is above the background. The numbers within each subsection of the plot indicates the fraction of the parent population.

(C) The fluorescence threshold for the synthetic circuit calculated for each combination of promoter activation strength and time.

(D) The fraction of cells expressing dsRed in cells below dsRed threshold (column II in (B)) for each combination of promoter activation strength and time.

S3). To verify the copy number of the synthetic gene circuit, we performed qPCR-based transgene copy number analysis and verified that all of the clones as well as the control contain a single copy of the transgene (Figure S2).

Subsequently, we used the circuit monoclonal cell line to engineer a genetically identical control cell line that lacks the functional miRNA 3′ UTR targets (thus rendering the intragenic miRNA inactive). This ensures that we preserve the genomic background of the cell line carrying the integrated circuit. The modification was once again carried out using the CRISPR genome editing methodology, where SpCas9 was used to cleave dsRed 3′ UTR precisely on the miRNA target (Figure S1). Disruption of the miRNA target site relies on NHEJR to incorporate insertion/deletion (indels) at the site of DNA cleavage. The expectation is that AmCyan will be equivalent between the intragenic miRNA and control clones. Meanwhile, the removal of FF3 target on 3′ UTR of dsRed transcript should result in higher dsRed expression in the control cell line. We indeed observe recovery of dsRed signal after the removal of intragenic miRNA activity.

Intragenic miRNA-Mediated Host Repression Is a Robust Filter of Promoter Activity

The first observation comparing the intragenic clones to control is that when the promoter activity (mapped by AmCyan fluorescence) is below a certain threshold, the dsRed activity is abolished (Figures 2A and 2B). Beyond this threshold, dsRed protein is expressed and is able to accumulate, but the

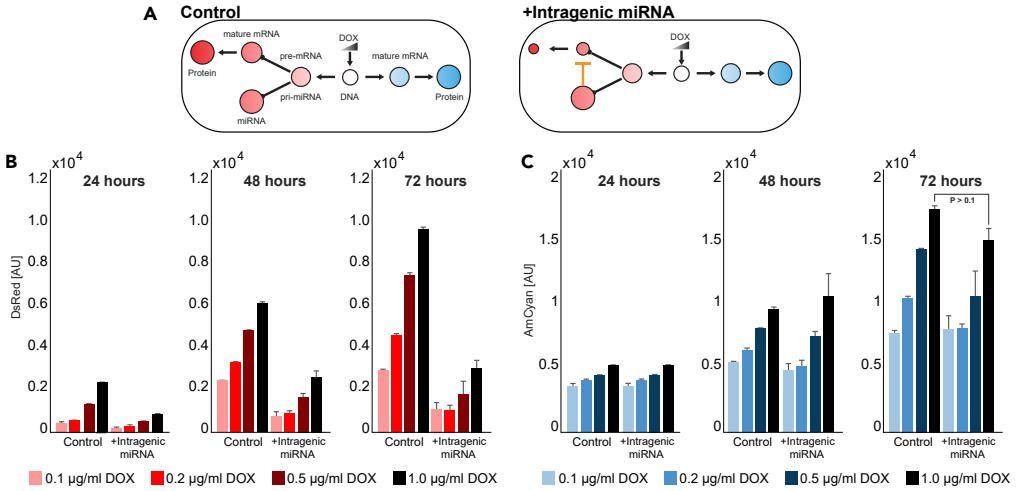

Figure 3. Expression Profile of Intragenic miRNA-Controlled Fluorescent Reporter

(A) Schematic representation of the control gene circuit (left) and the the circuit with intragenic miRNA-controlled dsRed (right). (B and C) Mean fluorescence of dsRed (B) and AmCyan (C) as measured by flow cytometry. The gene circuits were activated at four different doxycycline levels, and the fluorescence was captured at 24, 48, and 72 h.

maximum expression is lower than that of the control circuit. We devised a three-parameter piecewise function using our flow cytometry data (Figure S3, Transparent Methods). We fit this model to flow cytometry data collected from our circuit after induction at 0.1, 0.2, 0.5, and 1.0 µg/mL Dox and at 24, 48, and 72 h. Using the critical AmCyan values from our model fits, we defined an AmCyan region above background expression and below the threshold in which cells uniquely experience a dsRed suppression akin to filtering process, in which only cells expressing above the AmCyan threshold also express dsRed in the presence of miRNA regulation (Figures 2B, S4, and S5). We found that the critical AmCyan threshold value is independent of both time and doxycycline induction (Figure 2C), presumably because the thresholding effect is an intrinsic property of the intragenic miRNA action. We also provide the fraction of dsRed-positive cells within the AmCyan filtering region in both the intragenic miRNA and control cases (Figure 2D), again highlighting the filtering properties and their impact particularly at 48- and 72-hr measurements.

Characterization of the Circuit Output above the Threshold

We continued characterization of the circuit by measuring the reporter activity at various promoter activation strength and different times (Figure 3), above the filter threshold (Figures S6 and S7). In agreement with our expectations, the results show doxycycline-dependent increase for both reporters and comparable levels of expression for AmCyan. We observed a significant drop in dsRed expression for the active intragenic miRNA pathway as compared to the control cell line with the disrupted miRNA target.

As a control, we introduced antisense Morpholino (Kang et al., 2013; Summerton, 1999) oligomer to inhibit the miRNA post-transcriptionally and observe the recovery of dsRed expression and subsequent loss of threshold for dsRed expression as the system reached steady state (Figures S8 and S9). As an additional control, we ectopically introduced a third fluorescent protein (TagYFP) with FF3 miRNA target at the 3′ UTR and induce the circuit lacking the miRNA targets at various doxycycline concentrations (Figure S10). By introducing an independent reporter, we obtained the indirect measurement of the miRNA concentration, demonstrating proportionality between mature miRNA and mature mRNA (Figure S10C).

To investigate the clonal dependency of our circuit's operation, we isolated and examined two additional isogenic populations harboring our synthetic construct and repeated the same characterization process (Figure 4A). Flow cytometry results of all the new clones confirmed the expression relationships we observed previously, including the appearance of thresholding effect on dsRed transcript (Figures 4B and S7). All 4 populations show minimal differences in AmCyan expression (X axis) and a clear reduction in dsRed expression (Y axis) in the presence of active miRNA target, as indicated by the shaded 95%

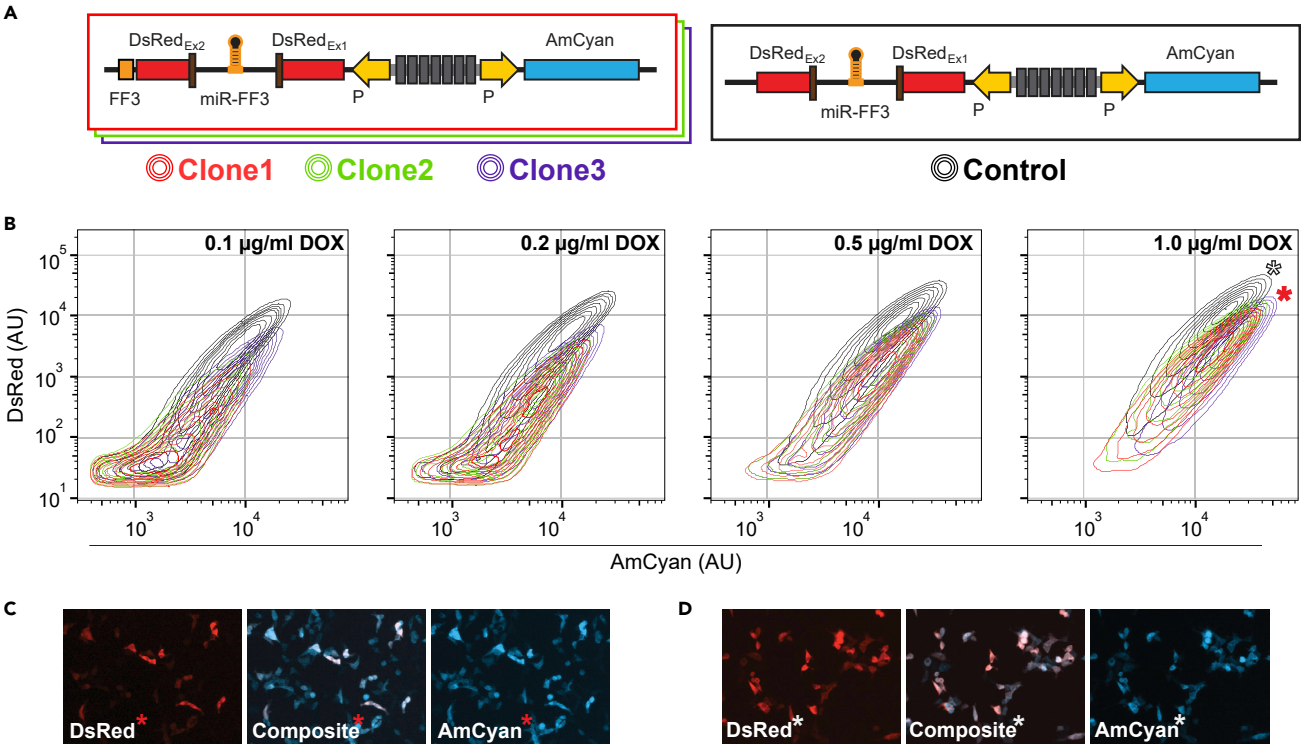

Figure 4. Induction and Characterization of the Intragenic microRNA and Control Architectures

(A) Schematic representation of the synthetic circuit with active intragenic miRNA-mediated transcriptional regulation (left) control circuit with removed FF3 miRNA target (right). Three isogenic clones of the synthetic circuit were used for subsequent characterization.

(B) Flow cytometry plots of dsRed and AmCyan expression captured at 48 h after various promoter activation strengths (i.e., doxycycline levels).

(C) Representative microscopy snapshots of the fluorescent reporters with active intragenic miRNA.

(D) Representative microscopy snapshots of the fluorescent reporters with inactive intragenic miRNA. Corresponding flow cytometry populations from panel B are denoted by *.

confidence interval (Figures 4B, S6, and S7). In addition, we provide representative fluorescent microscopy measurements at maximal promoter activation at 48 h (Figure 4C). Again, the disruption of miRNA target led to the co-expression of both fluorescent reporters (Figure 4D).

To study the dynamic behavior of our system, we obtained single-cell fluorescence measurements using time-lapse microscopy at a saturating doxycycline concentration (Figure S11). An image was captured every half hour for a 72-hr period, individual cells were identified and their integrated fluorescence was calculated for both AmCyan and dsRed (Figure S11A). Twenty cells were successfully tracked for longer than 35 h, and the fluorescence readings were plotted against time (Figure S11B). The inhibitory effect of repression via intragenic miRNA is observed from early stages of dsRed production and lasts throughout the 35-hr duration (Figure S11B left). The persistence of intragenic miRNA-mediated repression suggests that this mode of regulation reduces the total production capacity of the protein.

Impact of Intragenic miRNA-Mediated Silencing on Expression Noise

To examine how intragenic miRNA regulation and production effects the expression noise of the host gene, we calculated the mean and coefficient of variation (CV) of both the miRNA-containing host gene (dsRed) and the control output (AmCyan). We expect that higher doxycycline concentration and later measurement times to result in a lower measured CV as gene expression noise is known to scale inversely with protein abundance (Bar-Even et al., 2006; Blake et al., 2003; Elowitz et al., 2002). For each time point and doxycycline concentration, we plotted the CV of dsRed fluorescence against the mean dsRed fluorescence. We then grouped the data based on promoter activity (shaded area) and time (data color). Indeed, as the host gene is increasingly induced and its product accumulates in time, we observe that the host gene

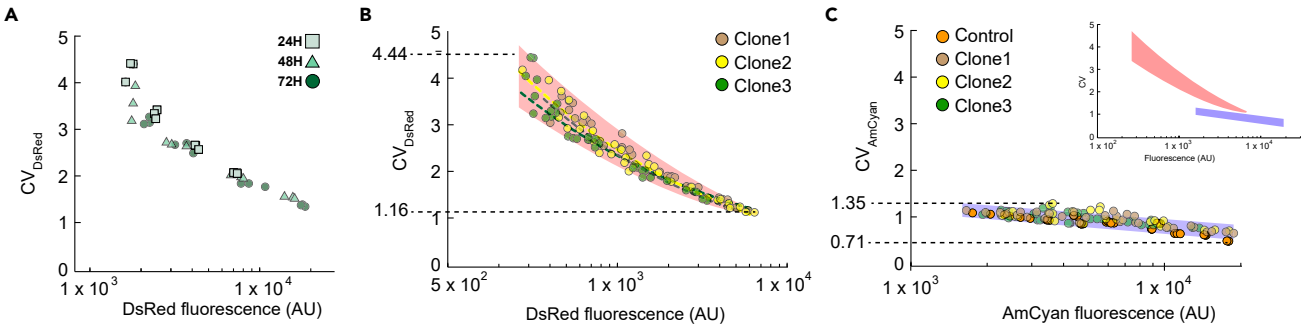

Figure 5. Intragenic miRNA-Mediation Results in Reduced Gene Single Reporter Expression and Noise

(A) Mean expressions of the fluorescent reporters are plotted against their respective noise (coefficient of variation) of the same population at various time points and promoter activation strengths (i.e., doxycycline concentration). As indicated by different colored boxes, data points are grouped by time after induction. Colors of discrete points indicate time points (24, 48, or 72 h), and the location within each box is indicative of the doxycycline concentration at the respective time point. Data in (A) show dsRed noise vs. mean plot of a single isogenic clone harboring active intragenic-miRNA for dsRed.

(B and C) Aggregated plot of dsRed (B) and AmCyan (C) noise vs. mean expression of each respective reporter from three different isogenic populations harboring the circuit with active DsRed-targeting intragenic miRNA. Plot for AmCyan includes control cell line with disrupted miRNA target for dsRed.

becomes less noisy in relation to its mean expression (Figure 5A). We also note that the variance of CV across replicates is highest at 24 h, and as the system reaches quasi-steady state, the population statistic becomes better defined. Eventually, the CV converges to a single value at 72 h. We observed same trend across all three clones (Figure 5B). The highest CV measured was from a population under the lowest concentration of doxycycline at 24 h, and the lowest CV was measured after 72 h at the saturating doxycycline concentration. Once again, the same trend was consistently observed across all three clones of the intragenic miRNA-containing host gene and the control (Figures 5B and 5C).

Our results also show that the mRNA/miRNA processing events have significant effect on expression noise, which tapers rapidly as proteins accumulate. Notably, we see that the intragenic miRNA-regulated protein's initially high noise, measured as a CV of 4.44, falls to a CV of 1.16 (Figure 5B) for high promoter activity. In contrast, AmCyan expression noise, which lacks splicing and microprocessing, falls from an initially lower CV of 1.35 to a CV of 0.71 (Figures 5C and S12) for high promoter activity. This is consistent with the notion that the coordinated process of splicing and miRNA processing (Pandya-Jones et al., 2013; Swinburne and Silver, 2008; Takashima et al., 2011) adds a layer of stochastic fluctuation to the transcription and the translation process (Herranz and Cohen, 2010; Komorowski et al., 2009; Marinov et al., 2014; Munsky et al., 2012; Paulsson, 2004; Waks et al., 2011).

Finally, we observe that the recovery of dsRed expression via removal of the microRNA target or sterically inhibiting its action is accompanied by corresponding increase in noise (Figures 6 and S13). Thus, we show that the inhibition of gene expression via intragenic miRNA reduces gene expression noise generated by the splicing and miRNA processing. Specifically, as illustrated in Figure 6, at comparable dsRed protein abundance, all three clones harboring the circuit with active intragenic miRNA pathway show decrease in noise compared to the control circuit.

DISCUSSION

While microRNAs have been studied thoroughly over the years and have been extensively used in synthetic biology applications, the effect that a miRNA's genetic origin has on its target mRNA's expression has yet to be distinguished. Here, we experimentally studied intragenic miRNA-mediated host transcript regulation (Bleris et al., 2011; Dill et al., 2012; Osella et al., 2011b), where the miRNA and its target are processed from the same gene transcript.

We demonstrate that this intragenic miRNA-mediated host transcript regulation simultaneously reduces both the noise and expression levels of the regulated host gene, a behavior not observed from miRNA that originates intergenically (Figure S14). Additionally, we demonstrate that the system behaves as a filter with a robust cutoff threshold. We have validated these claims with control experiments that each perturbs

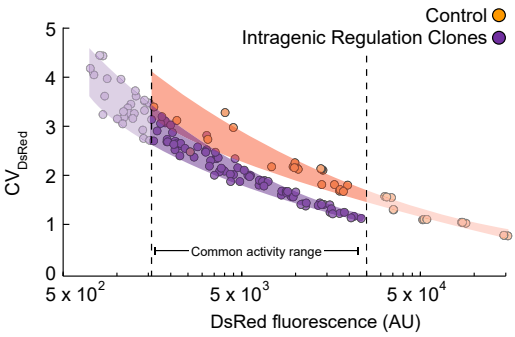

Figure 6. Intragenic miRNA Results in Reduced Expression and Noise

Aggregated plot of dsRed noise vs. mean expression for three isogenic clones with intragenic regulation (purple) and control population with disrupted miRNA target (orange). Data shown for each group include triplicate measurements of population induced with 0.1, 0.2, 0.5, and 1.0 μg/mL of doxycycline taken at 24, 48, and 72 h post induction.

different aspects of the circuit. Through these experiments, we reinforce the notion that properties of the intragenic-miRNA-regulated gene expression are unique to this particular mode of regulation (Figure S15).

Topologically, microRNA-mediated and other forms of single-edge repression of genes have been shown to increase expression noise as expression levels are reduced (Bar-Even et al., 2006; Hornung and Barkai, 2008; Komorowski et al., 2009; Paulsson, 2004). However, as part of a common network motif such as a negative feedback, single-edge repression can act to reduce noise in expression (Austin et al., 2006; Becskei and Serrano, 2000; Guinn and Balázsi, 2019; Shimoga et al., 2013). Our results suggest that by migrating the miRNA into the transcript of mRNA it represses, we generate an incoherent feedforward motif (Bleris et al., 2011; Lee et al., 2002; Mangan and Alon, 2003; Milo et al., 2002) that acts as a noise suppressant in addition to reducing expression levels. Intergenic miRNAs have been shown to efficiently abolish protein production below a fixed level of target mRNA, where this threshold shows a dependence on the relative amounts of miRNA and its mRNA target (Mukherji et al., 2011). Additionally, we have previously shown that the efficiency of miRNA repression nonlinearly depends on its genes induction strength and copy number (Quarton et al., 2018). By relocating a miRNA within the transcript of the gene in which it is repressing, we observe the emergence of a filtering behavior in which the cutoff threshold becomes independent of both its induction levels and time.

Advancements in the field of synthetic biology have produced circuits with increasingly sophisticated functions and a continually expanding library of components (Kitada et al., 2018; Lillacci et al., 2018; Ruder et al., 2011). As the field of synthetic biology moves toward clinical applications, precision and robustness become paramount. Herein, inspired by a naturally occurring architecture, we describe a compact and modular genetic circuit and demonstrate generally applicable properties of filtering and noise reduction.

Limitations of the Study

Here, we implement the intragenic miRNA-based host regulation in human cells and demonstrate its unique features using experimental results. Detailed mechanistic models and simulations can probe the specific biological processes responsible for the observed behavior. New architectures that incorporate different miRNAs and their targets can help generalize the results.

Resource Availability

Lead Contact

Further information and requests for resources and reagents should be directed to and will be fulfilled by the Lead Contact, Leonidas Bleris (bleris@utdallas.edu).

Materials Availability

Plasmids generated in this study are available from the Lead Contact with a completed Materials Transfer Agreement.

Data and Code Availability

The published article includes all data sets generated or analyzed during this study.

METHODS

All methods can be found in the accompanying Transparent Methods supplemental file.

SUPPLEMENTAL INFORMATION

Supplemental Information can be found online at https://doi.org/10.1016/j.isci.2020.101595.

ACKNOWLEDGMENTS

This work was funded by the US National Science Foundation (NSF) CAREER grant 1351354, NSF 1361355, a Cecil H. and Ida Green Endowment, the Eugene McDermott Graduate Fellows Program, and the University of Texas at Dallas.

AUTHOR CONTRIBUTIONS

T.K., K.E., and L.B. designed experiments. T.K., K.E., C.N., and Y.L. performed the experiments. T.K., T.Q. K.E., A.S., and L.B. analyzed the data. T.K., T.Q., and L.B. wrote the paper. L.B. supervised the project.

DECLARATION OF INTERESTS

The authors declare no competing interests.

Received: July 7, 2020
Revised: August 28, 2020
Accepted: September 16, 2020
Published: October 23, 2020

REFERENCES

Alon, U. (2006). An Introduction to Systems Biology: Design Principles of Biological Circuits (Chapman & Hall/Crc Mathematical and Computational Biology Series) ({Chapman & Hall/CRC}).

Austin, D.W., Allen, M.S., McCollum, J.M., Dar, R.D., Wilgus, J.R., Sayler, G.S., Samatova, N.F., Cox, C.D., and Simpson, M.L. (2006). Gene network shaping of inherent noise spectra. Nature *439*, 608–611.

Bar-Even, A., Paulsson, J., Maheshri, N., Carmi, M., O'Shea, E., Pilpel, Y., and Barkai, N. (2006). Noise in protein expression scales with natural protein abundance. Nat. Genet. *38*, 636–643.

Bartel, D.P. (2004). MicroRNAs: genomics, biogenesis, mechanism, and function. Cell *116*, 281–297.

Baskerville, S., and Bartel, D.P. (2005). Microarray profiling of microRNAs reveals frequent coexpression with neighboring miRNAs and host genes. RNA *11*, 241–247.

Becskei, A., and Serrano, L. (2000). Engineering stability in gene networks by autoregulation. Nature *405*, 590–593.

Blake, W.J., KÆrn, M., Cantor, C.R., and Collins, J.J. (2003). Noise in eukaryotic gene expression. Nature *422*, 633–637.

Bleris, L., Xie, Z., Glass, D., Adadey, A., Sontag, E., and Benenson, Y. (2011). Synthetic incoherent feedforward circuits show adaptation to the amount of their genetic template. Mol. Syst. Biol. *7*, 519.

Bosia, C., Osella, M., Baroudi, M., Corà, D., and Caselle, M. (2012). Gene autoregulation via intronic microRNAs and its functions. BMC Syst. Biol. *6*, 131.

Dill, H., Linder, B., Fehr, A., and Fischer, U. (2012). Intronic miR-26b controls neuronal differentiation by repressing its host transcript, ctdsp2. Genes Dev. *26*, 25–30.

Elowitz, M.B., Levine, A.J., Siggia, E.D., and Swain, P.S. (2002). Stochastic gene expression in a single cell. Science *297*, 1183–1186.

Flynt, A.S., and Lai, E.C. (2008). Biological principles of microRNA-mediated regulation: shared themes amid diversity. Nat. Rev. Genet. *9*, 831–842.

Guinn, M.T., and Balázsi, G. (2019). Noise-reducing optogenetic negative-feedback gene circuits in human cells. Nucleic Acids Res. *47*, 7703–7714.

He, C., Li, Z., Chen, P., Huang, H., Hurst, L.D., and Chen, J. (2012). Young intragenic miRNAs are less coexpressed with host genes than old ones: implications of miRNA–host gene coevolution. Nucleic Acids Res. *40*, 4002–4012.

Herranz, H., and Cohen, S.M. (2010). MicroRNAs and gene regulatory networks: managing the impact of noise in biological systems. Genes Dev. *24*, 1339–1344.

Hinske, L., Galante, P., Kuo, W., and Ohno-Machado, L. (2010). A potential role for intragenic miRNAs on their hosts' interactome. BMC Genomics *11*, 533.

Hinske, L.C., Franca, G.S., Torres, H.A.M., Ohara, D.T., Lopes-Ramos, C.M., Heyn, J., Reis, L.F.L., Ohno-Machado, L., Kreth, S., and Galante, P.A.F. (2014). miRIAD–integrating microRNA inter- and intragenic data. Database *2014*, bau099.

Hornung, G., and Barkai, N. (2008). Noise propagation and signaling sensitivity in biological networks: a role for positive feedback. PLoS Comput. Biol. *4*, e8.

Hsu, P.D., Lander, E.S., and Zhang, F. (2014). Development and applications of CRISPR-Cas9 for genome engineering. Cell *157*, 1262–1278.

Kang, T., White, J.T., Xie, Z., Benenson, Y., Sontag, E., and Bleris, L. (2013). Reverse engineering validation using a benchmark synthetic gene circuit in human cells. ACS Synth. Biol. *2*, 255–262.

Kashyap, N., Pham, B., Xie, Z., and Bleris, L. (2013). Transcripts for combined synthetic microRNA and gene delivery. Mol. Biosyst. *9*, 1919–1925.

Kim, Y.-K., and Kim, V.N. (2007). Processing of intronic microRNAs. EMBO J. *26*, 775–783.

Kitada, T., DiAndreth, B., Teague, B., and Weiss, R. (2018). Programming gene and engineered-cell therapies with synthetic biology. Science *359*, eaad1067.

Komorowski, M., Miękisz, J., and Kierzek, A.M. (2009). Translational repression contributes greater noise to gene expression than transcriptional repression. Biophys. J. *96*, 372–384.

Lee, T.I., Rinaldi, N.J., Robert, F., Odom, D.T., Bar-Joseph, Z., Gerber, G.K., Hannett, N.M., Harbison, C.T., Thompson, C.M., Simon, I., et al. (2002). Transcriptional regulatory networks in Saccharomyces cerevisiae. Science *298*, 799–804.

Lee, Y., Kim, M., Han, J., Yeom, K.-H., Lee, S., Baek, S.H., and Kim, V.N. (2004). MicroRNA genes are transcribed by RNA polymerase II. EMBO J. *23*, 4051–4060.

Leisner, M., Bleris, L., Lohmueller, J., Xie, Z., and Benenson, Y. (2010). Rationally designed logic integration of regulatory signals in mammalian cells. Nat. Nanotechnol. *5*, 666–670.

Li, M., Fu, W., Wo, L., Shu, X., Liu, F., and Li, C. (2013). miR-128 and its target genes in tumorigenesis and metastasis. Exp. Cell Res. *319*, 3059–3064.

Li, S.-C., Tang, P., and Lin, W.-C. (2007). Intronic MicroRNA: discovery and biological implications. DNA Cell Biol *26*, 195–207.

Lillacci, G., Benenson, Y., and Khammash, M. (2018). Synthetic control systems for high performance gene expression in mammalian cells. Nucleic Acids Res. *46*, 9855–9863.

Lutter, D., Marr, C., Krumsiek, J., Lang, E.W., and Theis, F.J. (2010). Intronic microRNAs support their host genes by mediating synergistic and antagonistic regulatory effects. BMC Genomics *11*, 224.

Ma, N., Wang, X., Qiao, Y., Li, F., Hui, Y., Zou, C., Jin, J., Lv, G., Peng, Y., Wang, L., et al. (2011). Coexpression of an intronic microRNA and its host gene reveals a potential role for miR-483-5p as an IGF2 partner. Mol. Cell. Endocrinol. *333*, 96–101.

Mangan, S., and Alon, U. (2003). Structure and function of the feed-forward loop network motif. Proc. Natl. Acad. Sci. U S A *100*, 11980–11985.

Marinov, G.K., Williams, B.A., McCue, K., Schroth, G.P., Gertz, J., Myers, R.M., and Wold, B.J. (2014). From single-cell to cell-pool transcriptomes: stochasticity in gene expression and RNA splicing. Genome Res. *24*, 496–510.

Milo, R., Shen-Orr, S., Itzkovitz, S., Kashtan, N., Chklovskii, D., and Alon, U. (2002). Network motifs: simple building blocks of complex networks. Science *298*, 824–827.

Mukherji, S., Ebert, M.S., Zheng, G.X.Y., Tsang, J.S., Sharp, P.A., and van Oudenaarden, A. (2011). MicroRNAs can generate thresholds in target gene expression. Nat. Genet. *43*, 854–859.

Munsky, B., Neuert, G., and van Oudenaarden, A. (2012). Using gene expression noise to understand gene regulation. Science *336*, 183–187.

Osella, M., Bosia, C., Corá, D., and Caselle, M. (2011a). The role of incoherent microRNA-mediated feedforward loops in noise buffering. PLoS Comput. Biol. *7*, e1001101.

Osella, M., Bosia, C., Corá, D., and Caselle, M. (2011b). The role of incoherent MicroRNA-mediated feedforward loops in noise buffering. PLoS Comput. Biol. *7*, e1001101.

Pandya-Jones, A., Bhatt, D.M., Lin, C.-H., Tong, A.-J., Smale, S.T., and Black, D.L. (2013). Splicing kinetics and transcript release from the chromatin compartment limit the rate of Lipid A-induced gene expression. RNA *19*, 811–827.

Paulsson, J. (2004). Summing up the noise in gene networks. Nature *427*, 415–418.

Qi, L.S., Larson, M.H., Gilbert, L.A., Doudna, J.A., Weissman, J.S., Arkin, A.P., and Lim, W.A. (2013). Repurposing CRISPR as an RNA-guided platform for sequence-specific control of gene expression. Cell *152*, 1173–1183.

Quarton, T., Ehrhardt, K., Lee, J., Kannan, S., Li, Y., Ma, L., and Bleris, L. (2018). Mapping the operational landscape of microRNAs in synthetic gene circuits. Npj Syst. Biol. Appl. *4*, 6.

Rinaudo, K., Bleris, L., Maddamsetti, R., Subramanian, S., Weiss, R., and Benenson, Y. (2007). A universal RNAi-based logic evaluator that operates in mammalian cells. Nat. Biotechnol. *25*, 795–801.

Rodriguez, A., Griffiths-Jones, S., Ashurst, J.L., and Bradley, A. (2004). Identification of mammalian microRNA host genes and transcription units. Genome Res. *14*, 1902.

Ruder, W.C., Lu, T., and Collins, J.J. (2011). Synthetic biology moving into the clinic. Science *333*, 1248–1252.

Sadelain, M., Papapetrou, E.P., and Bushman, F.D. (2012). Safe harbours for the integration of new DNA in the human genome. Nat. Rev. Cancer *12*, 51–58.

Satoh, W., Hirai, Y., Tamayose, K., and Shimada, T. (2000). Site-specific integration of an adeno-associated virus vector plasmid mediated by regulated expression of. Rep. Based Cre-loxP Recombination *74*, 10631–10638.

Shimoga, V., White, J.T., Li, Y., Sontag, E., and Bleris, L. (2013). Synthetic mammalian transgene negative autoregulation. Mol. Syst. Biol. *9*, 670.

Summerton, J. (1999). Morpholino antisense oligomers: the case for an RNase H-independent structural type. Biochim. Biophys. Acta - Gene Struct. Expr. *1489*, 141–158.

Swinburne, I.A., and Silver, P.A. (2008). Intron delays and transcriptional timing during development. Dev. Cell *14*, 324–330.

Takashima, Y., Ohtsuka, T., Gonzalez, A., Miyachi, H., and Kageyama, R. (2011). Intronic delay is essential for oscillatory expression in the segmentation clock. Proc. Natl. Acad. Sci. *108*, 3300–3305.

Waks, Z., Klein, A.M., and Silver, P.A. (2011). Cell-to-cell variability of alternative RNA splicing. Mol. Syst. Biol. *7*, 506.

Ying, S.-Y., and Lin, S.-L. (2006). Current perspectives in intronic micro RNAs (miRNAs). J. Biomed. Sci. *13*, 5–15.

iScience, Volume *23*

Supplemental Information

Robust Filtering and Noise Suppression in Intragenic miRNA-Mediated Host Regulation

Taek Kang, Tyler Quarton, Chance M. Nowak, Kristina Ehrhardt, Abhyudai Singh, Yi Li, and Leonidas Bleris

Reference	Sequence
sgRNA 1 (5')	**AGCTTGTCGACGATATCTCC**
sgRNA 2 (3')	**CAAACGATATGGGCTGAATAC**
FF3 target	**TTTGCTATACCCGATCTTA**

Figure S1. Guide RNA sequences for removing FF3 miRNA targets. Related to Figure 1**.** In order to remove the FF3 miRNA target in the genomically-integrated synthetic circuit, the nuclease was targeted directly to the target site with 2 different sgRNAs. The sgRNA targets are shown in green brackets.

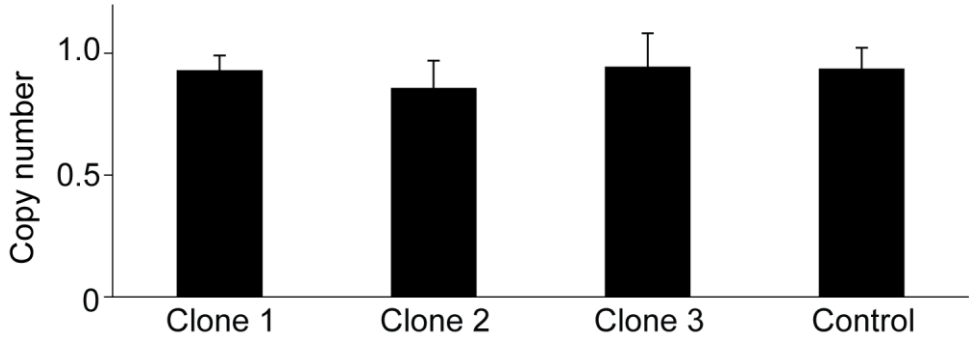

Figure S2. Calculated copy numbers for each transgenic clones and control. Related to Transparent Methods.

For each stable clone, 50 ng of genomic DNA were used performed and the average copy numbers were calculated as the mean ± SD. For statistical analysis, z scores were calculated against estimated integer copy numbers, and $-1.96<z<1.96$ was determined as no statistical difference (corresponding to 95% confidence interval).

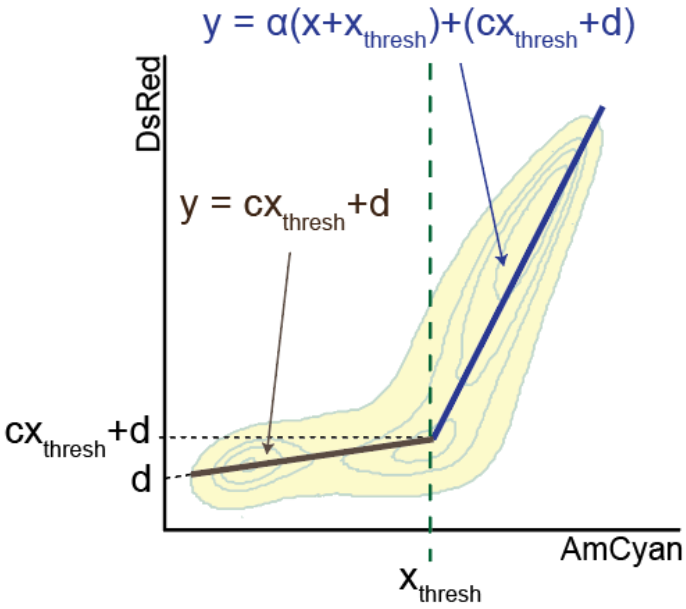

Figure S3. Graphical illustration of the promoter activity threshold calculation. Related to Figure 2. Flow cytometry population of the stable cell lines can be separated into population above and below the DsRed expression threshold (x_{thresh}). Each of these populations can be described by a linear curve after fitting.

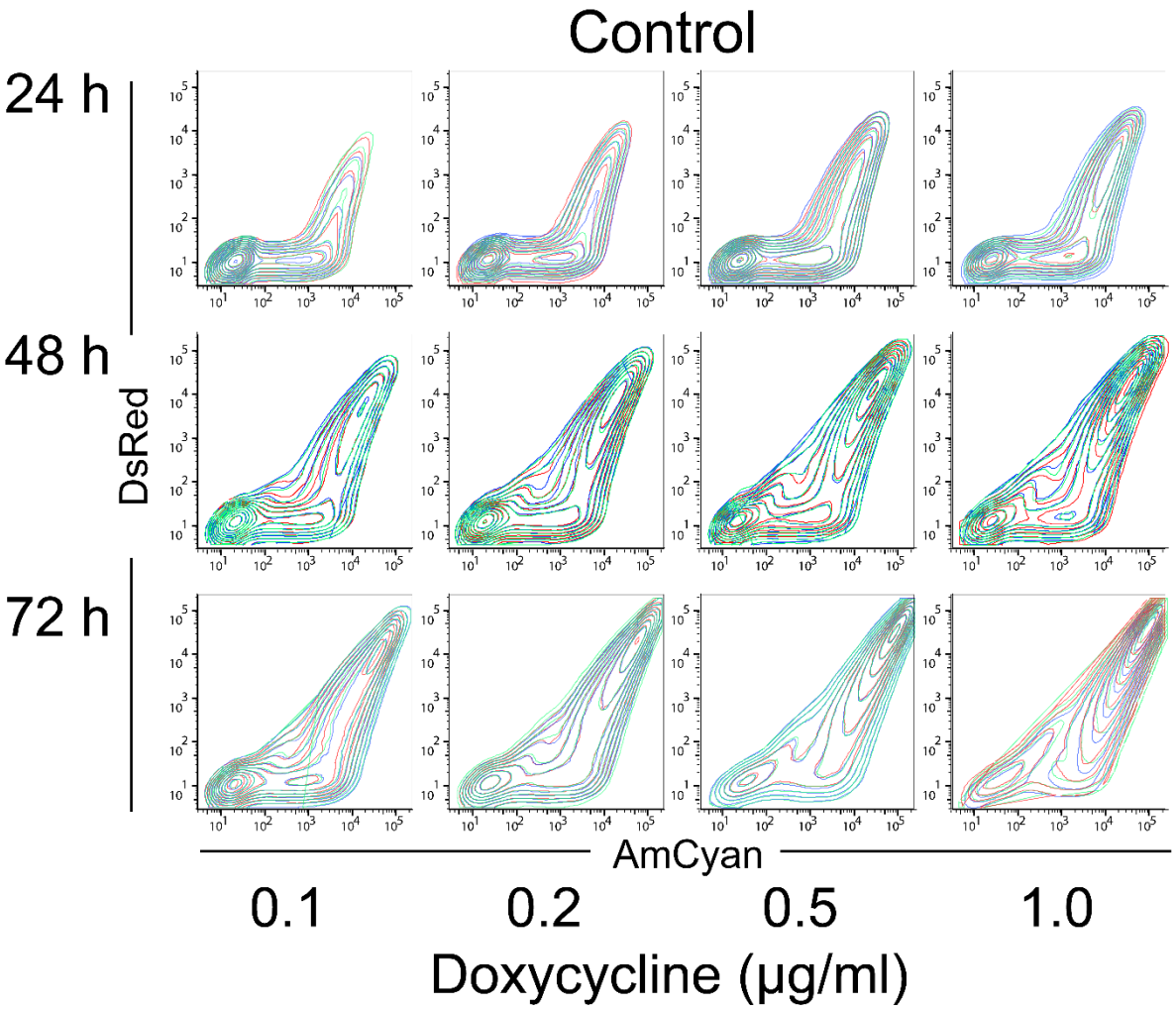

Figure S4. Flow cytometry measurement of populations without intragenic miRNA regulated DsRed. Related to Figure 2. Each panel contains the triplicates indicated by green, red and blue contours.

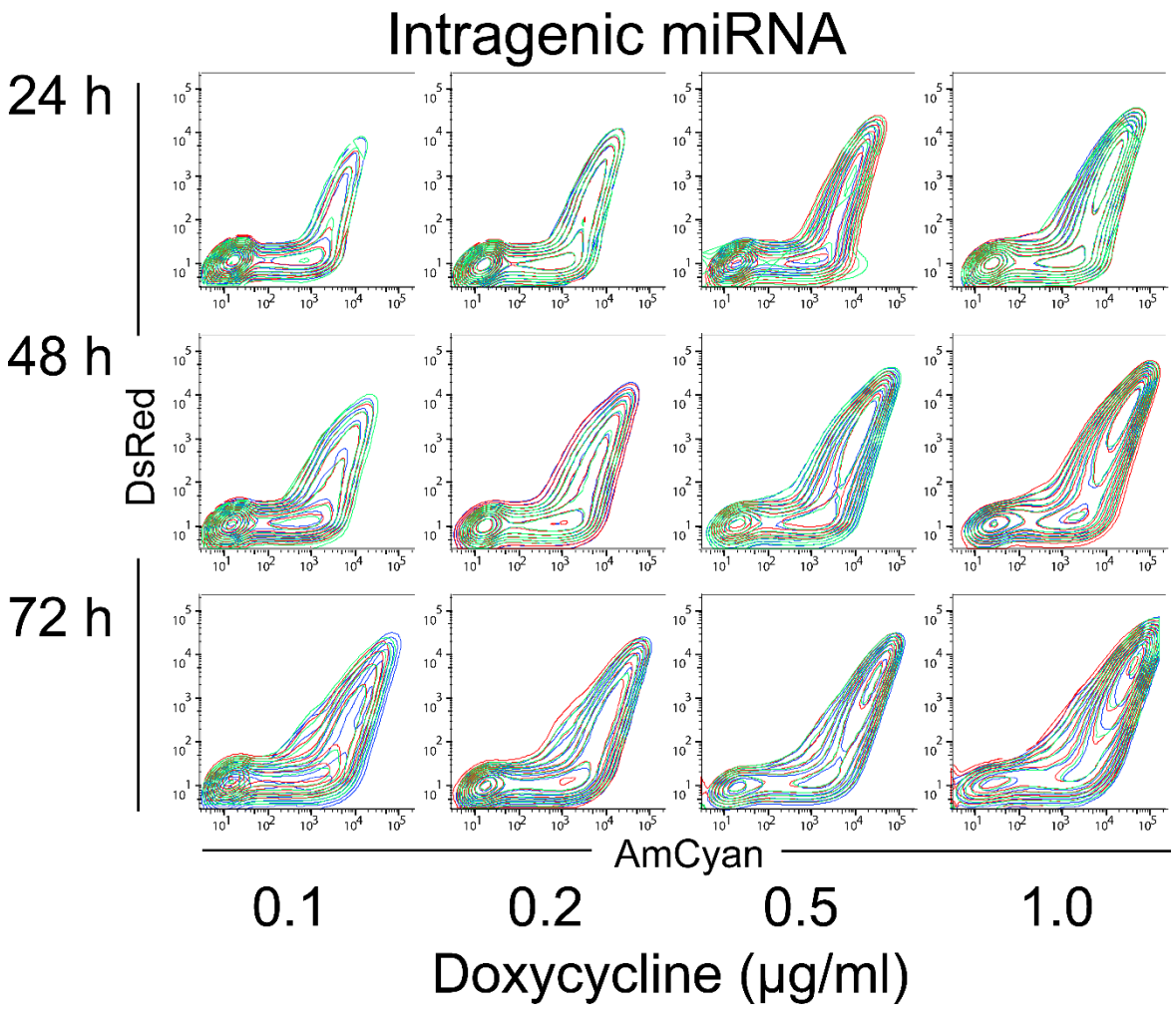

Figure S5. Flow cytometry measurement of populations intragenic miRNA regulated DsRed. Related to Figure 2**.** Each panel contains the triplicates indicated by green, red and blue contours.

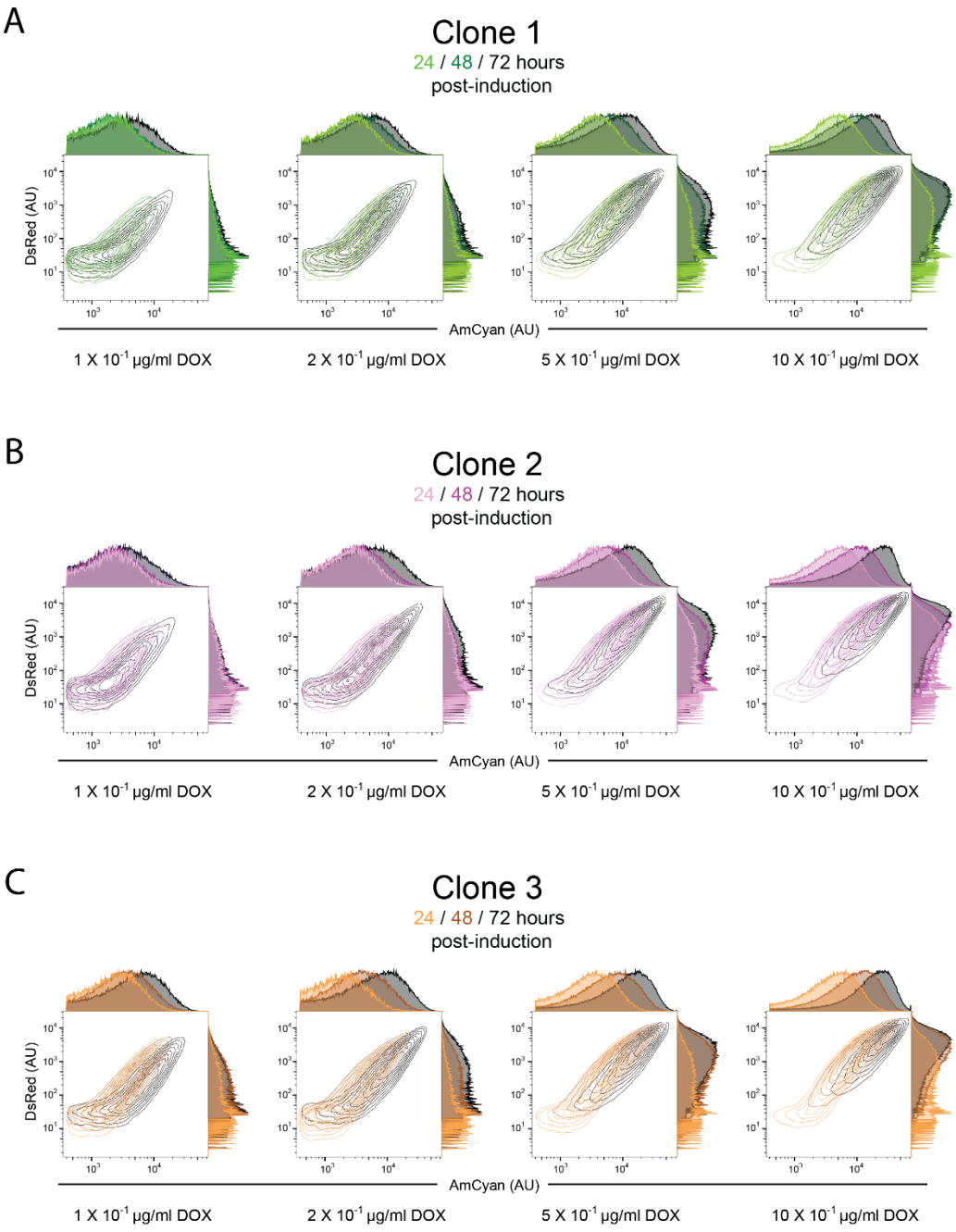

Figure S6. Doxycycline titration of the synthetic gene circuit for three isogenic clones. Related to Figure 3. For each isogenic clones containing the synthetic gene circuit, the fluorescent reporter expression was analyzed at 4 different doxcycyline levels (0.1, 0.2, 0.5, 1.0 µg, left to right, respectively) at 24, 48 and 72 hours.

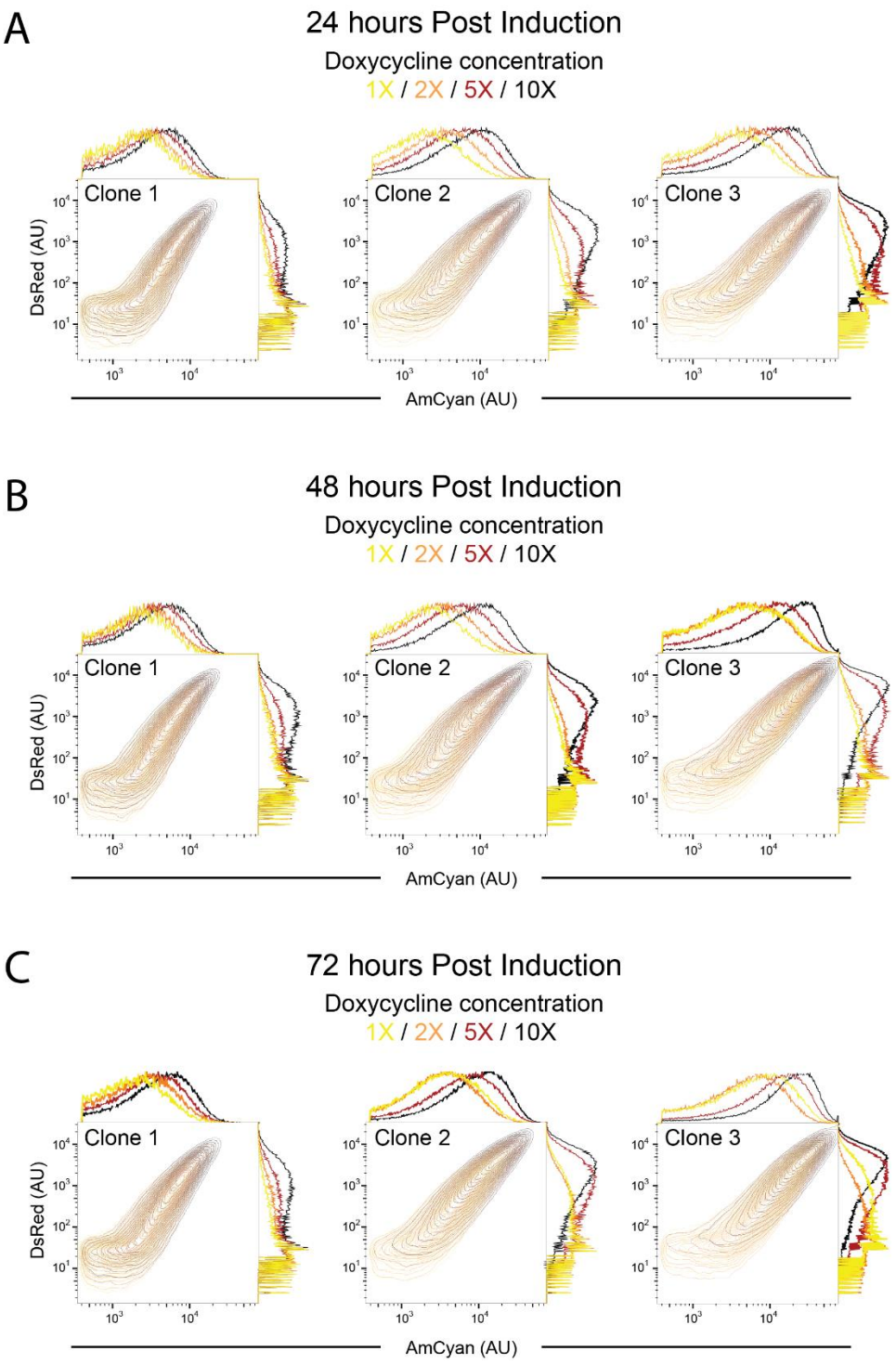

Figure S7. Doxycycline titration of the synthetic gene circuit for three different time points. Related to Figure 3. See Figure S6 for description. Doxycycline concentrations of 1X, 2X, 5X,10X correspond to 0.1, 0.2, 0.5, 1.0 µg, respectively).

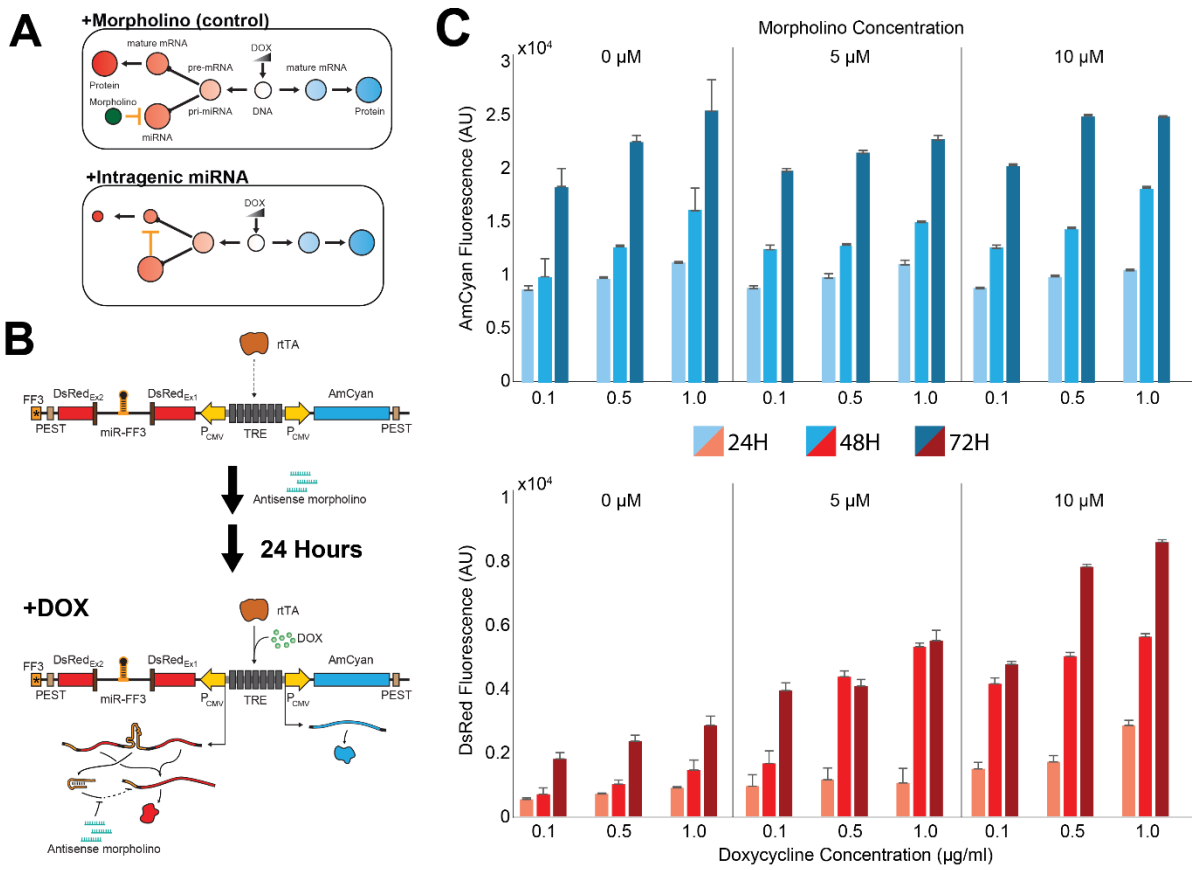

Figure S8. Steric inhibition of intragenic FF3 miRNA action via Morpholino. Related to Figure 4. (A) Morpholino oligomers are nucleic acid analogs that sterically inhibit RNA activity. (B) Customized Morpholino oligomers antisense to mature FF3 miRNA were introduced 24 hours to the cell lines harboring the synthetic construct. (C) Flow cytometry results of the circuits 24, 48, and 72 hours after induction.

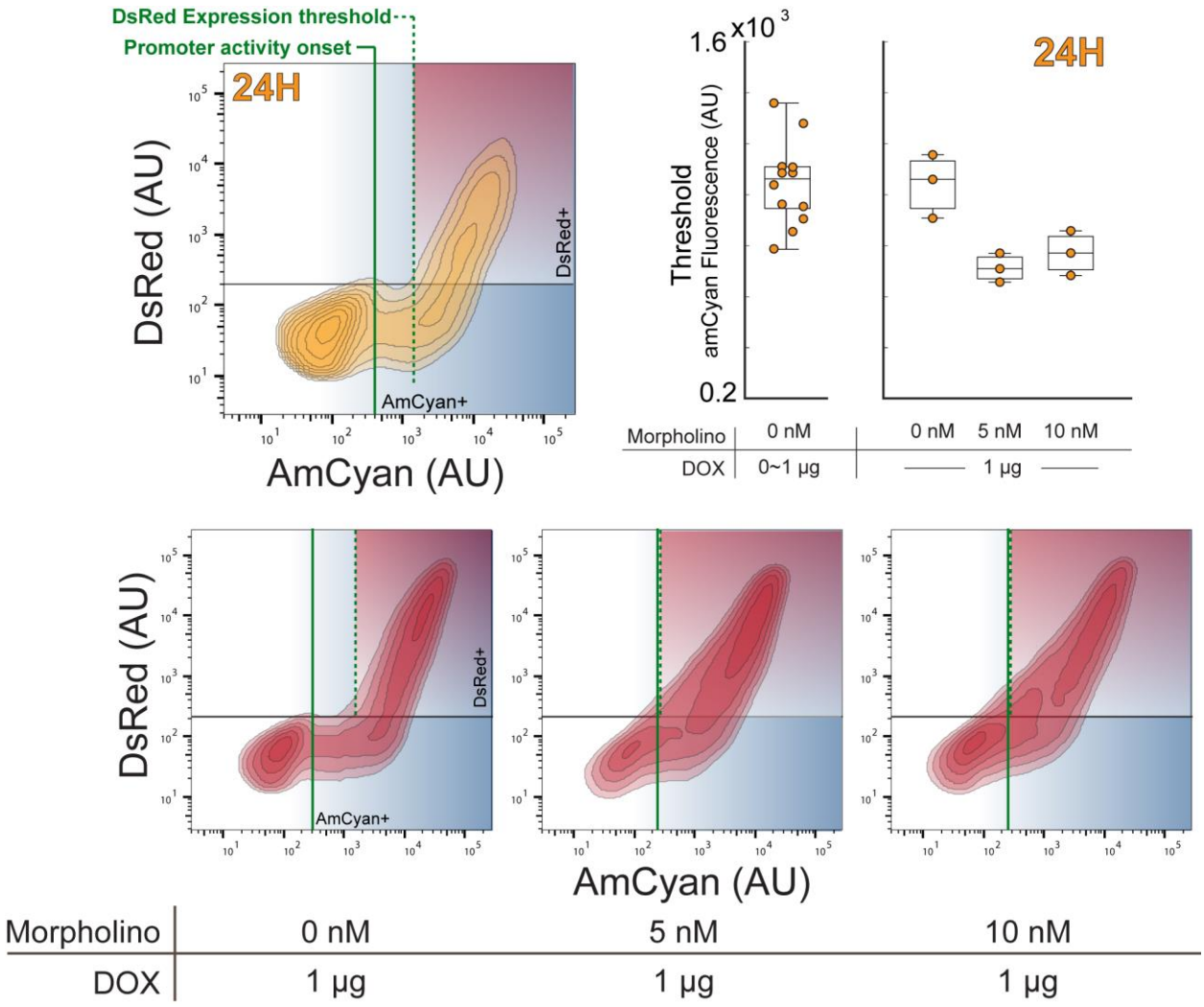

Figure S9. Steric inhibition of intragenic FF3 miRNA action via Morpholino alters DsRed expression threshold. Related to Figure 2. With intragenic miRNA regulation, the threshold promoter activity required for active DsRed expression, as indicated by AmCyan fluorescence, (green dotted line, top left) is reached after the onset of promoter activity (green solid line). This threshold decreases with the addition of Morpholino oligomer 24 hours after induction (top right). The boxplot on the left indicates data presented in the Figure 2C. Eventually, measured at 48h and 72h, the threshold disappears and DsRed expression is observed immediately at the onset of promoter activity (bottom).

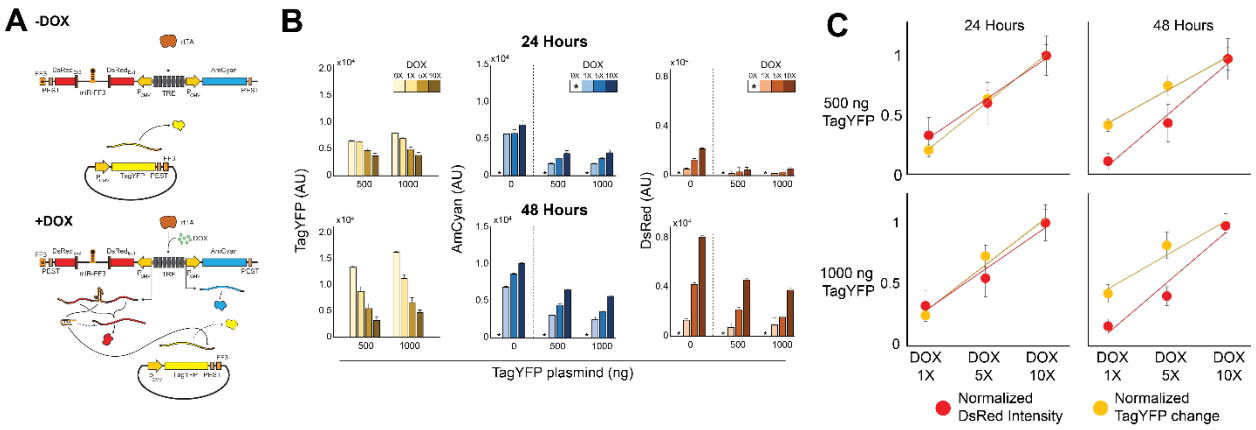

Figure S10. Isolated effect of intragenic FF3 miRNA, as measured by an independent fluorescent reporter. Related to Figure 4. (A) TagYFP fluorescent reporter plasmid with constitutive expression was introduced to the control circuit where DsRed FF3 target has been scrambled (top). Once induced, the mature FF3 miRNA directly effects TagYFP production. (B) Fluorescence of cells expressing all three fluorescent reporters. (C) DsRed fluorescence intensity at each doxycycline concentration plotted alongside the magnitude of decrease in TagYFP at the corresponding doxycycline concentration.

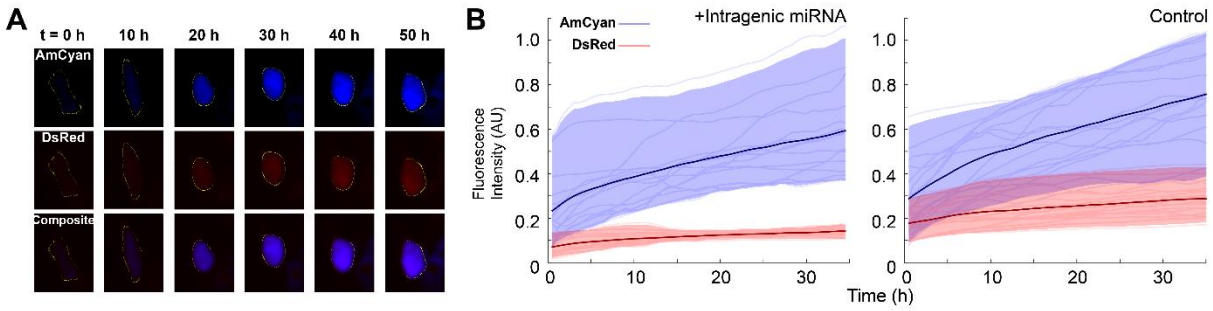

Figure S11. Single-cell time lapse microscopy of the synthetic circuit. Related to Figure 4. Fluorescence activity of cells harboring the synthetic gene circuit were captured every 30 minutes for 72 hours. (A) Snapshots of representative fluorescent microscopy images. Rows represent fluorescence of each cells and columns represent various time points. (B) Plot composed of 20 individual traces single-cells tracked minimum of 35 hours. Dark colored line and the shaded area indicates mean fluorescence intensity and 95% confidence interval for each time point.

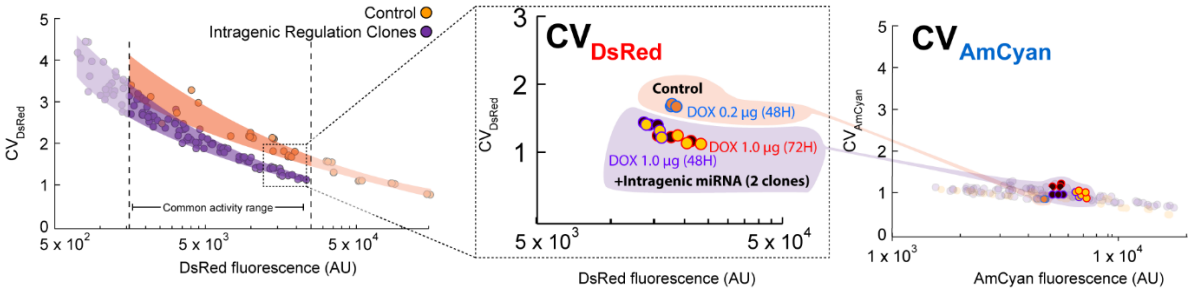

Figure S12. Comparison of fluorescent reporter noises at a given DsRed fluorescence. Related to Figure 5. Noise of expression in DsRed for all doxycycline concentration and time (left). Doxycycline concentration and time period for comparable expression but different noise for DsRed expression (center). Noise of AmCyan expression for corresponding population (right).

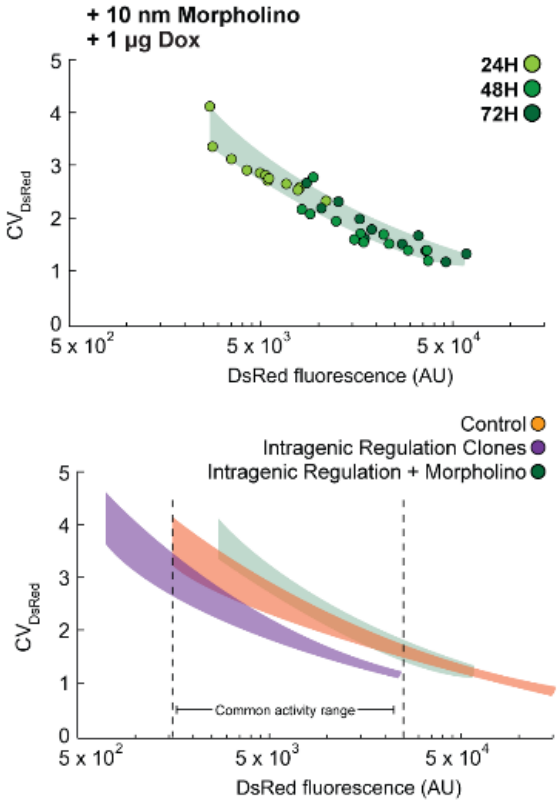

Figure S13. Steric inhibition of intragenic FF3 miRNA action via Morpholino reduces expression noise. Related to Figure 6. Mean expression of the DsRed plotted against the coefficient of variation. Aggregated plot of DsRed noise vs. mean expression for three isogenic clones with intragenic regulation (purple), control population with disrupted miRNA target (orange) and Morpholino (green).

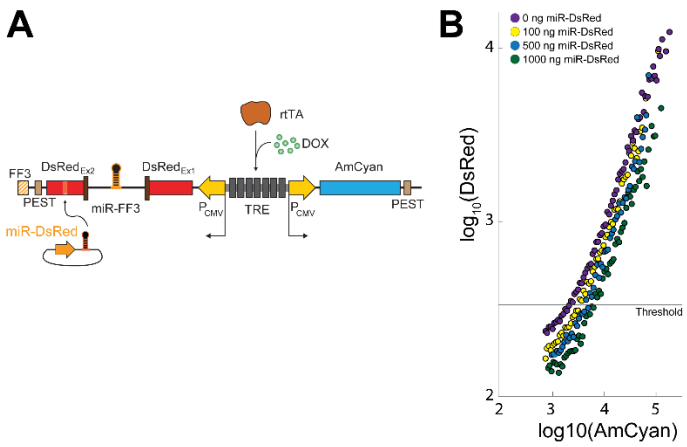

Figure S14. Effect of intergenic miRNA targeting DsRed. Related to Figure 2. (A) The stable cell line with scrambled FF3 miRNA was transfected with varying amounts of constitutively-expressed miRNA expression plasmid. The intergenic miRNA is fully complementary to the exon of DsRed. The promoter was induced with a saturating concentration of doxycycline (1 µg/ml) and the fluorescence was measured 48 hours post induction. (B) Scatter plot representing the flow cytometry results of the experiment. Each data point represents a mean fluorescence of the binned population. Increasing amounts of intergenic miRNA plasmid causes the AmCyan threshold for a given DsRed expression to increase.

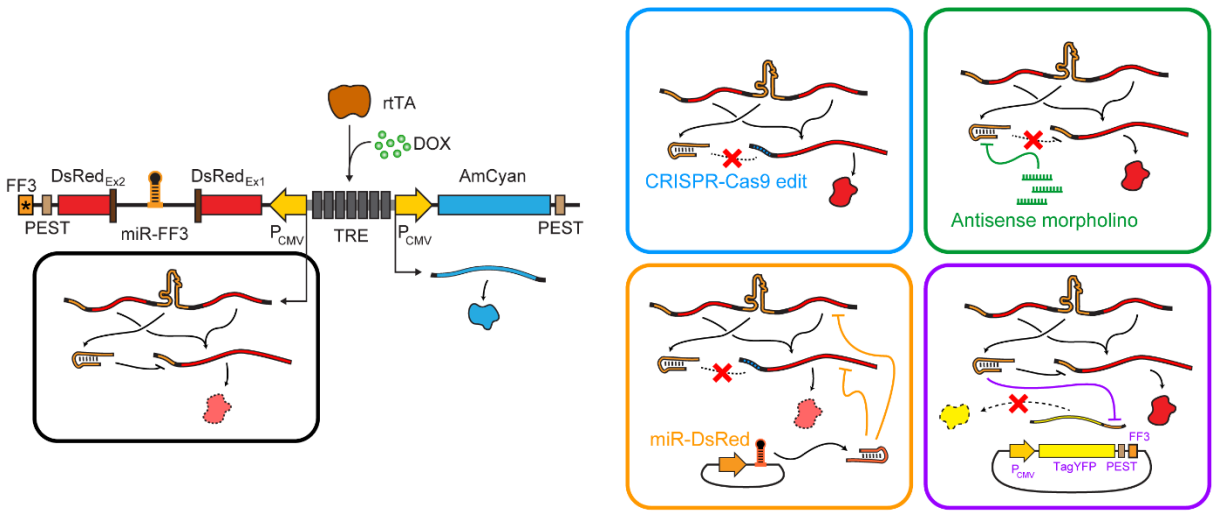

Circuit Type Modification	Experimental Active intragenic miR	Control Disrupted miR target	Morpholino Steric miR blocking	DsRed miRNA Intergenic miRNA
Presence of a threshold	Yes	Yes	Yes	No
Threshold robustness	Yes; to time and dox	No	No	N/A
Noise	Low	High	High	N/A

Figure S15. Summary of control experiments performed for intragenic miRNA and subsequent effect on threshold and noise. Related to Figure 1. DsRed expression noise was not calculated for the experimental diagram shown in the purple box. The detailed results of this experiments are shown in Figure S12.

List of intragenic miRNAs		
Known protein-coding genes		20 530
Known miRNA precursors		1871
	Intragenic miRNAs	**1072**
	Host genes	930
	Sense miRNAs in respect to host orientation	902
	Antisense miRNAs in respect to host orientation	170
	Intergenic miRNAs	**799**
Expressed coding genes		18 442
Expressed miRNAs		1111

Table S1. Distribution of intragenic miRNAs in human genome. Related to Figure 1. (Hinske et al., 2014)

Left homology arm from the adeno-associated virus integration site (5' HA)	GAGCACTTCCTTCTCGGCGCTGCACCACGTGATGTCC TCTGAGCGGATCCTCCCCGTGTCTGGGTCCTCTCCGG GCATCTCTCCTCCCTCACCCAACCCCATGCCGTCTTC ACTCGCTGGGTTCCCTTTTCCTTCTCCTTCTGGGGCCT GTGCCATCTCTCGTTTCTTAGGATGGCCTTCTCCGAC GGATGTCTCCCTTGCGTCCCGCCTCCCCTTCTTGTAG GCCTGCATCATCACCGTTTTTCTGGACAACCCCAAAGT ACCCCGTCTCCCTGGCTTTAGCCACCTCTCCATCCTC TTGCTTTCTTTGCCTGGACACCCCGTTCTCCTGTGGAT TCGGGTCACCTCTCACTCCTTTCATTTGGGCAGCTCC CCTACCCCCCTTACCTCTCTAGTCTGTGCTAGCTCTTC CAGCCCCCTGTCATGGCATCTTCCAGGGGTCCGAGA GCTCAGCTAGTCTTCTTCCTCCAACCCGGGCCCCTAT GTCCACTTCAGGACAGCA
Right homology arm from the adeno-associated virus integration site (3' HA)	ACTAGGGACAGGATTGGTGACAGAAAAGCCCCATCCT TAGGCCTCCTCCTTCCTAGTCTCCTGATATTGGGTCTA ACCCCCACCTCCTGTTAGGCAGATTCCTTATCTGGTG ACACACCCCCATTTCCTGGAGCCATCTCTCTCCTTGC CAGAACCTCTAAGGTTTGCTTACGATGGAGCCAGAGA GGATCCTGGGAGGGAGAGCTTGGCAGGGGGTGGGA GGGAAGGGGGGGATGCGTGACCTGCCCGGTTCTCAG TGGCCACCCTGCGCTACCCTCTCCCAGAACCTGAGCT GCTCTGACGCGGCCGTCTGGTGCGTTTCACTGATCCT GGTGCTGCAGCTTCCTTACACTTCCCAAGAGGAGAAG CAGTTTGGAAAAACAAAATCAGAATAAGTTGGTCCTGA GTTCTAACTTTGGCTCTTCACCTTTCTAGTCCCCAATTT ATATTGTTCCTCCGTGCGTCAGTTTTACCTGTGAGATA AGGCCAGTAGCCAGCCCCGTCCTGGCAGGGCTGTGG TGAGGAGGGGGGTGTCCGTGTGGAAAACTCCCTTTGT GAGAATGGTGCGTCCTAGGTGTTCACCAGGTCGTGGC CGCCTCTACTCCCTTTCTCTTTCTCCATCCTTCTTTCCT TAAAGAGTCCCCAGTGCTATCTGGGACATATTCCTCC GCCCAGAGCAGGGTCCCGCTTCCCTAAGGCCCTGCT CTGGGCTTCTGGGTTTGAGTCCTTGGCAAGCCCAGGA GAGGCGCTCAGGCTTCCCTGTCCCCCTTCCTCGTCCA CCATCTCATGCCCCTGGCTCTCCTGCCCCTTCCCTAC AGGGGTTCCTGGCTCTGCTCT
AAVS1-specific sgRNA	GTCCCCTCCACCCCACAGT

Table S2. Integration of the circuit plasmid into AAVS1 locus. Related to Figure 1. Left and right homology arm of the plasmid used to gnomically integrate synthetic construct, and the AAVS1-specific sgRNA used to induce NHEJ.

DsRed forward	5’-ctccaccacggtgtagtcct-3’
DsRed reverse	5’-agaccgtgtacaaggccaag-3’
BRCA1 forward	5’-gagcgtcccctcacaaataa-3’
BRCA1 reverse	5’-tgctccgtttggttagttcc-3’

Table S3. **Primers used for qPCR-based transgene copy number validation.** Related to Figure 1.

Transparent Methods

Cell Culture: Tet-On cells and the derived stable clones were maintained at 37°C, 5% CO_2 and 100% humidity. The cells were grown in Dulbecco's modified Eagle's medium (DMEM, Life Technologies, #11965-118) supplemented with 10% Fetal Bovine Serum (FBS, Atlanta Biologicals, #S11550), 0.1 mM MEM non-essential amino acids (Life Technologies, #11140-050), 0.045 units/mL of Penicillin and 0.045 units/mL of Streptomycin (Penicillin-Streptomycin liquid, Life Technologies, #15140-122). To pass the cells, the adherent culture was washed with DPBS (Dulbecco's Phosphate-Buffered Saline, 1X with calcium and magnesium, Corning, #21-030-CM) and then trypsinized with Trypsin-EDTA (Trypsin-EDTA (0.25%), phenol red, Life Technologies, #25200-114) and finally diluted in fresh medium upon reaching 50–90% confluence. The derived stable cells were maintained in 2ug/mL puromycin.

Generation of stable cell line: To generate the monoclonal stable cell lines, ~10 million of the Tet-On cells were seeded onto a 10 cm petri dish. 16 hours later, the cells were transiently transfected with 5 μg of the donor plasmid, 5 μg of the U6-gRNA-PCMV-Cas9-t2A-mKate plasmid using the JetPRIME reagent (Polyplus Transfection). 48 hours later, puromycin (Life Technologies, catalog number: A1113803) was added at the final concentration of 2 μg/mL. The selection lasted ~2 weeks, after which the surviving clones were pooled to generate the polyclonal stable cells, from which monoclonal stable cells were isolated using the serial dilution method.

Fluorescence Microscopy: Microscopy was performed 24–72 hours post induction with doxycycline. The live cells were grown on 12-well plates (Greiner Bio-One) in the complete medium. Cells were imaged using an Olympus IX81 microscope in a Precision Control environmental chamber. The images were captured using a Hamamatsu ORCA-03 Cooled monochrome digital camera. The filter sets (Chroma) are as follows: ET436/20x (excitation) and ET480/40 m (emission) for AmCyan, ET545/30x (excitation) and ET620/60 m (emission) for DsRed. Data collection and processing was performed in the software package Slidebook 5.0. All images within a given experimental set were collected with the same exposure times and underwent identical processing.

Time-Lapse Fluorescence Microscopy: Microscopy was performed immediately following induction with doxycycline. The live cells were grown on 6-well plates (Greiner Bio-One) in the complete medium. Cells were imaged using Zeiss Axio Observer Z1 microscope in a Incubation control environmental chamber. The images were captured using an Andor iXon X3 camera. The CoolLED pE-2 lasers were used for excitation. The filter sets (Semrock) are as follows: 438/24 (excitation) and 483/32 (emission) for AmCyan, 543/22 (excitation) and 593/40 (emission) for DsRed. Data collection was performed using Micro-Manager 1.4. Image processing was performed in ImageJ. All images were collected with the same exposure times and underwent identical processing.

Flow Cytometry: Flow cytometry was performed 24-72 hours post induction with doxycycline. Each well of the 12-well plates were washed with 1.0 mL of DPBS and then trypsinized with 0.3 mL 0.25% Trypsin-EDTA at 37°C for 5 minutes. Trypsin-EDTA was then neutralized by adding 0.7 mL of complete medium. The cell suspension was centrifuged at 1,000 rpm for 5 minutes and after removal of supernatants, the cell pellets were resuspended in 0.5 mL DPBS. The cells were analyzed on a BD LSRFortessa flow analyzer. AmCyan was measured with a 445-nm laser, a 505

long-pass filter, and 525/50 band-pass filter, and DsRed with a 561-nm laser, and 582/15 band-pass filter. For all experiments ~200,000 events were collected. All wells within a given experimental set had the same number of events collected with the same voltages and underwent identical processing. The flow cytometry data was processed using FlowJo. A FSC (forward scatter)/SSC (side scatter) gate was generated applied to all cell samples. The gated cells were then further gated into AmCyan positive cells by gating above the AmCyan levels of uninduced cells. For some analysis a DsRed positive gate was then applied, again by gating above the DsRed levels of uninduced cells. All data underwent identical processing for each analysis.

Single Cell Serial Dilution: To generate clonal population, serial dilution method used with a 96-well plate. First, a confluent cell culture was detached using trypsin and resuspended using conditioned media. The conditioned media prepared by harvesting at approximately 75% confluency, then clarified by centrifugation at 1000 x g for 10 minutes then passed through a sterile filter. Resuspension was diluted to a final concentration of 2 x 10 4 cells/mL, then added inoculated to a single well in a 96-well plate.

Minimum Promoter Activity Threshold: To model this thresholding relationship between the intragenic miRNA-regulated DsRed and the unregulated AmCyan using flow cytometry data, we devised a three-parameter piecewise function of the form

$$\mu(x) = \begin{cases} c\,x + d & x \leq x_{thresh} \\ a\,(x - x_{thresh}) + (c\,x_{thresh} + d) & x > x_{thresh} \end{cases}, \quad (1)$$

where μ represents the miRNA repressed DsRed expression, x represents the unregulated AmCyan expression, x_{thresh} captures the critical point in which active DsRed expression begins and a represents the proportionality between DsRed and AmCyan above the AmCyan threshold. The parameters c and d each represent slope and y-intercept of the linear curve that describes the cytometry population below the promoter theshold **(Figure S2)**. Operationally, the promoter threshold is an inflection point at which the slope of the curve describing the cytometry population changes. The curve beyond the inflection point ($x > x_{thresh}$) can be now described with the equation $a\,(x - x_{thresh}) + (c\,x_{thresh} + d)$ this curve, where a is the slope of this curve. This can be described as a three-parameter piecewise function as shown below:

$$y = \begin{cases} c\,x + d & x \leq x_{thresh} \\ a\,(x - x_{thresh}) + (c\,x_{thresh} + d) & x > x_{thresh} \end{cases}$$

The x_{thresh} that satisfies the above function corresponds to the promoter threshold value, i.e. the expression of AmCyan at which the observable DsRed production begins. In order to find x_{thresh}, we use Mathematica function NonlinearModelFit with the piecewise function as the desired output form. The process cycles through iterations of nonlinear regression fitting procedure until the result reaches 95% confidence, i.e. there is a 95% probability that the population lies within the confidence interval.

Transgene copy number validation: Real-time quantitative PCR (qPCR) has been recognized as a viable alternative to Southern blot or fluorescence *in situ* hybridization for evaluation of gene copy numbers (Hoebeeck et al., 2007). As such, we performed real-time quantitative PCR to determine the absolute copies of integration for our circuits using $\Delta\Delta C_t$ method **(Table S3)**. The HEK293 cell line that was previously verified to contain a single copy of DsRed transgene was

used as the control cell line (Shimoga et al., 2013). All genomic DNA samples were extracted using DNeasy Blood and Tissue kit (Qiagen).

Briefly, the procedure for determining the copy number is as follows: Harvest genomic DNA for the transgenic clones as well as the control cell line, perform qPCR and obtain the C_t values for each stable clone for the transgene (DsRed) and the endogenous reference gene (BRCA1), calculate the copy number with $2^{-\Delta\Delta Ct} = ((1 + E_{DsRED})^{-\Delta Ct,DsRED}) / ((1 + E_{BRCA1})^{-\Delta Ct,\ BRCA1})$, where E_{DsRED} is the PCR amplification efficiency for DsRed (1.07) and E_{BRCA1} for endogenous reference gene BRCA1 (0.98) (Zheng et al., 2011) (**Figure S2)**.

Supplementary References

Hinske, L.C., Franca, G.S., Torres, H.A.M., Ohara, D.T., Lopes-Ramos, C.M., Heyn, J., Reis, L.F.L., Ohno-Machado, L., Kreth, S., and Galante, P.A.F. (2014). miRIAD--integrating microRNA inter- and intragenic data. Database *2014*, bau099–bau099.

Hoebeeck, J., Speleman, F., and Vandesompele, J. (2007). Real-time quantitative PCR as an alternative to southern blot or fluorescence in situ hybridization for detection of gene copy number changes. Methods Mol. Biol. *353*, 205–226.

Shimoga, V., White, J.T., Li, Y., Sontag, E., and Bleris, L. (2013). Synthetic mammalian transgene negative autoregulation. Mol. Syst. Biol. *9*, 670.

Zheng, S., Houseman, E.A., Morrison, Z., Wrensch, M.R., Patoka, J.S., Ramos, C., Haas-Kogan, D.A., McBride, S., Marsit, C.J., Christensen, B.C., et al. (2011). DNA hypermethylation profiles associated with glioma subtypes and EZH2 and IGFBP2 mRNA expression. Neuro. Oncol. *13*, 280–289.